Compact Thermally Tunable Silicon Wavelength Switch: Modeling and Characterization

Xuan Wang, Jose A. Martinez, Magdalena S. Nawrocka, *Member, IEEE*, and Roberto R. Panepucci, *Member, IEEE*

***Abstract*—A wavelength-selective photonic switch is developed based on a Si microring resonator using thermooptic effect. The 10-μm-diameter microring resonator uses single-mode strip Si waveguides of dimension 0.25 μm $\times$ 0.45 μm operating at 1.5 μm. Full-width at half-maximum are in the range 0.1–0.2 nm. The ultrawide tunable range (>6.4 nm) and wide free spectral range ($\sim$18 nm) of the switch element enables wavelength reconfigurable multichannel matrix switch by wavelength multiplexing/demultiplexing. Average rise delay time of 14 μs with low switching power of 3.15 mW has been achieved with 0.2-nm wavelength tuning and 78 μs, 104 mW for 6.4-nm tuning. Fall delay times are usually less than 10 μs. Thermal simulations show 10%–20% agreement with the measurements up to 3.2-nm tuning. The compact size of the switch shows its potential as an active element in photonic integrated circuits.**

***Index Terms*—Microring resonator, silicon-on-insulator (SOI), thermooptic effect, wavelength tuning.**

I. Introduction

MICRORING resonators are multifunctional photonic elements with many device applications such as filters [1], multiplexers [2], and modulators [3], making use of their high wavelength selectivity. As microring resonators integrated with silicon-on-insulator (SOI) technology, they are very promising for photonic integrated circuits. Because of the large refractive index difference between Si ($n = 3.48$) and SiO_2 ($n = 1.46$), the SOI technology allows submicrometer single-mode waveguides. This ensures ultrahigh light confinement leading to compact photonic devices with sharp bends, making possible large-scale photonic integration [4]. While thermooptic tuning has moderate speed compared with electrooptic [3] and all-optic tuning [5], with silicon's high thermooptic coefficient, a much wider wavelength tunable range can be realized. The large tunable range and large free spectral range (FSR) of the silicon microring resonator has enabled a wavelength reconfigurable multichannel matrix switch [6].

In this letter, we investigate in detail the thermal tuning time response of a 10-μm-diameter SOI-based ring resonator with FSR of 18 nm and full-width at half-maximum (FWHM) in the range 0.1–0.2 nm. This is achieved through the use of a local microheater to tune the resonance wavelength to a target signal wavelength. By using several input and output rings on a common bus waveguide, with corresponding heaters, multiple signals can be multiplexed/demultiplexed. A 1×4 wavelength reconfigurable switch prototype has been realized in our previous work using this approach [6]. In this work, we demonstrate wide-range wavelength tuning (6.4 nm) enabling a compact 32×32 matrix switch with 0.2-nm channel spacing. Thermal simulations indicate key parameters for designing devices with higher switching speed, lower power consumption, and reduced size.

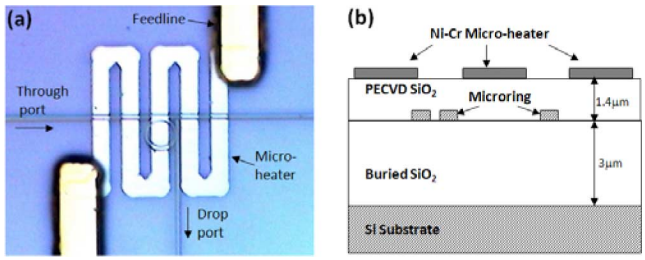

Fig. 1. (a) Top view microscopic picture of fabricated switch element; (b) schematic of the cross section at the ring.

II. Experiment and Simulation

Fig. 1(a) shows the top view microscopic image of the fabricated switch element, with a signal coupled from the through port to the drop port of the switch. The cross section of the element is also shown on Fig. 1(b). The single-mode SOI strip waveguides have the dimension of 0.45 μm in width and 0.25 μm in height. The fabrication began with an SOI wafer with 3-μm buried oxide layer and 0.25-μm silicon layer. The waveguide pattern was defined by ebeam lithography with 5-nm beam steps into hydrogen silsesquioxane resist and transferred by reactive ion etching process. Etching was followed by deposition of $\sim$1.4 μm top cladding using the plasma-enhanced chemical vapor deposition process. Then the $\sim$0.1-μm Ni–Cr microheater was generated through a process sequence of photolithography, thermal deposition, and liftoff. The microheater size is 50 μm$\times$ 50 μm. The Ti–Au contact pads and feed lines were generated by the same sequence except deposited by sputtering. Finally, the input and output waveguides are all polished to the edge of the chip where waveguides are finished with nanotapers, which can theoretically reduce insertion loss to below 1 dB [7].

The characterization of a single switch element was performed by a tunable laser (Ando 4321D) with tunable range of 1520–1620 nm. Tapered fiber launches light into the input through port of the switch. The transmitted light from the drop port of the switch element was collected by an objective lens

Manuscript received December 4, 2007; revised February 13, 2008. This work was supported in part by the AFOSR under FA9550-05-1-0232, New Span Opto-Technology Inc. and National Science Foundation Award 0446571.

The authors are with the Department of Electrical and Computer Engineering, Florida International University, Miami, FL 33174 USA (e-mail: panepucc@fiu.edu).

Color versions of one or more of the figures in this letter are available online at http://ieeexplore.ieee.org.

Digital Object Identifier 10.1109/LPT.2008.922907

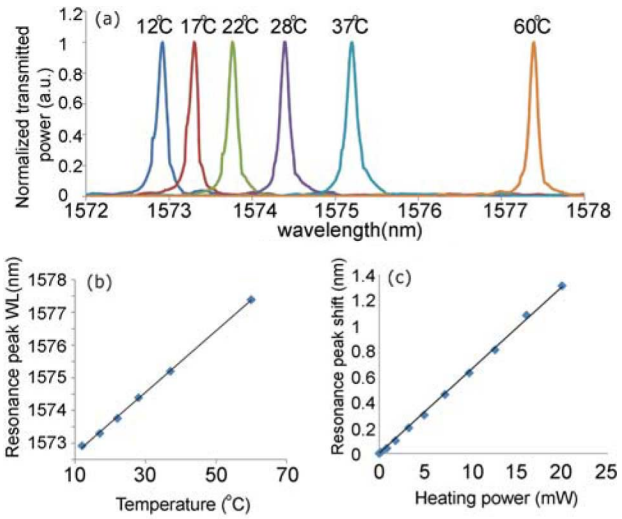

Fig. 2. (a) Normalized transmitted power spectra at different temperatures; (b) resonance peak wavelength versus temperature with linear fit; (c) resonance shift versus electrical power applied on the microheater with linear fit.

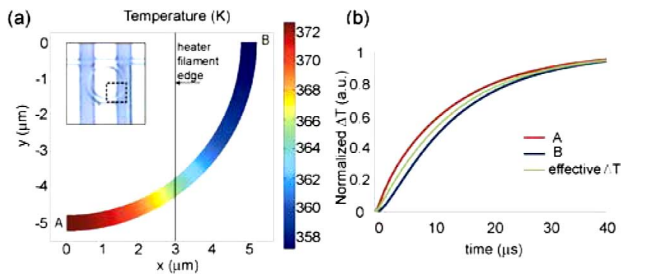

Fig. 3. (a) Simulated temperature distribution on the quarter of microring when resonance tuned to target wavelength $\lambda_t = 1580.29$ nm (room temperature resonance peak $\lambda_0 = 1573.89$ nm). (b) Normalized DT time response of point A and B on plot (a) and effective DT of the whole ring.

and detected by a Newport 818-IR photodetector after a polarizer which only allows light with TE (E-field parallel to device plane) polarization pass through. We consider TE mode only as the narrow resonance characteristics for the TE polarization (FWHM $= 0.1$–0.2 nm) allow more nonoverlapping channels within the tunable range. To drive the microheater on top of the ring, two electrical probes were used to provide ohmic contact to the pads with negligible induced resistance compared to the microheater. The probes are connected to a voltage source which provides heating current.

A Peltier thermoelectric module attached to the bottom of the chip was used to accurately characterize the drop port transmission spectra of the ring resonator at different equilibrium temperatures (from 12 °C to 60 °C). Drop port spectra are shown in Fig. 2(a), and the temperature dependence of the TE resonance peak shifts is shown in Fig. 2(b). We determined the linear resonance shift coefficient to be 0.095 nm $^\circ\mathrm{C}^{-1}$ consistent with the thermooptic coefficient of Si of 1.51×10^{-4} $^\circ\mathrm{C}^{-1}$ (assuming $n_{\mathrm{eff}} = 2.5$), similar to reported values [8]. For our microheaters, data was taken under constant current injection at thermal equilibrium condition. The heater resistance was determined to be $\sim$800 Ω. Fig. 2(c) indicates the linear relationship of resonance wavelength shift as a function of applied electrical power. A low switching power of 3.15 mW was needed for 0.2-nm wavelength tuning with 104.3 mW needed for 6.4-nm shift.

To understand the switching response, 3-D finite-element thermal simulations were performed to model temperature profile and transient during switching processes. The simulations assume perfect heat sink on the back of the chip and uniform and constant heat flux from the heater element covered area during heating. The resonance wavelength can be determined giving initial resonance wavelength and temperature difference (ΔT) distribution along the ring by applying the measured thermooptic coefficient. To eliminate feed line effects, the heat flux was set to the value that tunes the specific resonance wavelength (λ_0) at room temperature (set to 295 K) to the predefined target resonance wavelengths (λ_t) to thermal equilibrium state during heating. Fig. 3(a) shows the temperature distribution along the quarter ring when the resonance is tuned from $\lambda_0 = 1573.89$ nm to $\lambda_t = 1580.29$ nm (a 6.4-nm resonance shift). The temperature distribution is assumed to be symmetrical about both X and Y axis. A significant temperature gradient of $\sim$15 °C is observed between the hottest and coolest spots, marked as "A" and "B" on Fig. 3(a). The resonance wavelength shift $(\Delta\lambda)$ was calculated by integrating the induced refractive index change $(\Delta n\ (T))$ along the ring. An effective ΔT was defined as the temperature change that results in the same $\Delta\lambda$ for a uniform temperature change along the ring. Fig. 3(b) shows different temporal responses between "A" and "B" as well as the effective ΔT time response, and not surprisingly it falls between both curves. We found that the nonuniform heating of the ring causes an additional delay to the time response.

The thermal switching of the microring filter between λ_0 and λ_t is characterized by four time constants. During heating we observe detuning from λ_0, and tuning to λ_t; while during the cooling cycle, the detuning from λ_t, and tuning to λ_0. A probe signal at the target wavelength was used to measure the tuning and detuning waveforms when a 100-Hz square wave voltage with 10% "on" duty cycle was applied to the microheater. The voltage amplitude of the square wave was set to the desired wavelength shift. The period was significantly longer than the switching time, which allows equilibrium to be reached during both "heater on" periods and "heater off" (cooling) periods. This measurement was carried out for six wavelength shift values, for three different resonant peaks. Fig. 4 shows a typical switch response, for switching between $\lambda_t = 1574.69$ nm and $\lambda_0 = 1573.89$ nm $(\Delta\lambda = 0.8$ nm) in (c) and (d) respectively, with heating power shown in (a). Fig. 4(b) shows the simulated time response of the resonance peak wavelength calculated from the temperature simulation. Using a Lorentzian lineshape at the peak wavelength, we obtained the simulated power at λ_t and at λ_0, shown in Fig. 4(c) and (d), respectively.

Measurements were carried out setting $\Delta\lambda$ to multiples of channel spacing, namely 0.2, 0.4, 0.8, 1.6, 3.2, and 6.4 nm. Fig. 5 shows the rise/fall delay time as a function of $\Delta\lambda$ for three resonance peaks at 1573.89, 1592.65, and 1611.80 nm (room temperature). The rise/fall delay time (τ_{dr}/τ_{df}) for the tuning/detuning process is defined as the time between the heating power

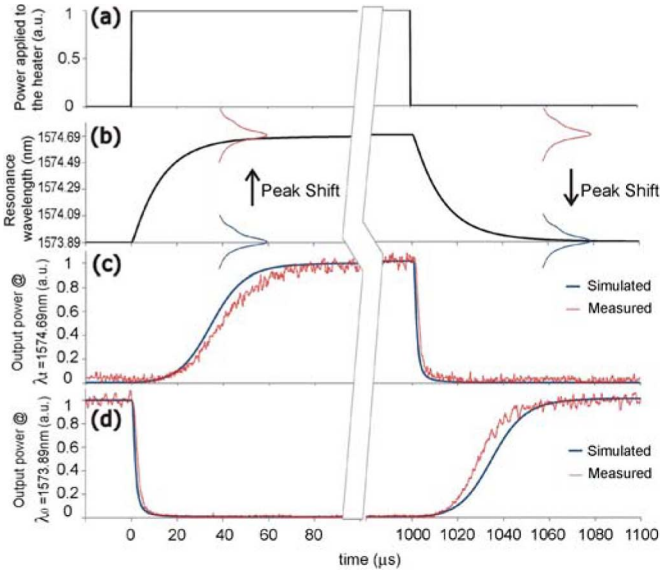

Fig. 4. (a) Normalized power applied to the heater; (b) simulated peak wavelength of the tuning resonance. Simulated and measured output power transient at (c) $\lambda_t = 1574.69$ nm and (d) $\lambda_0 = 1573.89$ nm.

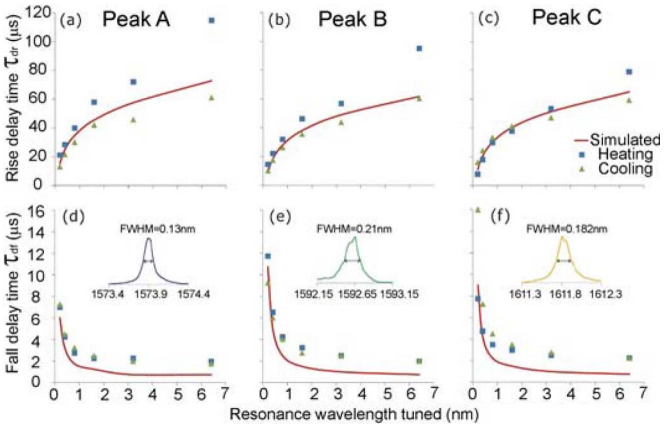

Fig. 5. Plots of tuning rise delay times of room-temperature resonance peaks at (a) 1573.89 nm (Peak A), (b) 1592.65 nm (Peak B), and (c) 1611.80 nm (Peak C) as well as plots of fall delay times of the peaks (d), (e), and (f), respectively. The curves are simulated results and the symbols are measured values. The insets are the corresponding peak spectra. Note the different time scale between rise and fall plots.

on/off time and the photodetector voltage signal rising/falling to 50% of the maximum power.

Calculation of the rise/fall delay time response of the device from simulations requires knowledge of the half-width at half-maximum (HWHM) power point only. We used 50% of the measured FWHM to calculate the expected rise/fall delay times (τ_{dr}/τ_{df}) from the simulated temperature response. The calculated results are shown in Fig. 5 as lines.

III. Discussion

As shown in Fig. 5, the rise/fall times are in very good agreement with the simulated values. For different resonance peaks of the same ring, the simulated switching times are different due to the slightly different HWHM, in spite of the same temperature time response. The fall times (the detuning process) are typically much shorter than the rise (tuning) times, due to the initial rapid motion of the Lorentzian peak position as seen in Fig. 4(b). On the other hand, the quasi-exponential nature of the temperature tuning to the final value, either through cooling or heating, leads to a slow natural log trend for higher resonance shifts. The cooling and heating rise-delay times are not identical due to the asymmetry of the measured lineshape (HWHM), as seen in the inset of Fig. 5(d)–(f). Furthermore, a stronger deviation from the simulated values can be seen in the high resonance shift region, when tuning by heating as seen in Fig. 5(a)–(c). The ∼0.2-nm tuning from approximately 0%–100% signal occurs in the last 3% of the temperature range. Parasitic feedline heating, imperfect heat sinking, convection or perhaps strain-induced anisotropy effects could also be the cause, and deserve further exploration. The measured fall times are in good agreement with the simulation, being higher than the simulation due to the ∼1 μs photodetector rise/fall time.

IV. Conclusion

We have demonstrated a compact (active area of $\sim 10\ \mu\text{m} \times 10\ \mu\text{m}$) tunable wavelength switch with ultrawide tunable range (>6.4 nm) which enables multichannel switching/routing. Our simulations accurately predicted the characteristics of the switch, with no adjustable parameters. They already indicate a ∼40% faster switch with a reduced top cladding thickness of 0.5 μm. Another finding is that uniform heating over the silicon ring increases speed. Improved power consumption is expected for smaller ring diameters, such as those in [8] with 2-μm radius and ∼47-nm FSR. The devices had rise-delay times of 10–120 μs, and fall-delay times of less than 16 μs for a switching range of 0.2–6.4 nm.

References

[1] B. E. Little, S. T. Chu, H. A. Haus, J. Foresi, and J.-P. Laine, "Microring resonator channel dropping filters," *J. Lightw. Technol.*, vol. 15, no. 6, pp. 998–1005, Jun. 1997.

[2] B. E. Little, S. T. Chu, P. P. Absil, J. V. Hryniewicz, F. G. Johnson, F. Seifert, D. Gill, V. Van, O. King, and M. Trakalo, "Very high-order microring resonator filters for WDM applications," *IEEE Photon. Technol. Lett.*, vol. 16, no. 10, pp. 2263–2265, Oct. 2004.

[3] Q. Xu, B. Schmidt, S. Pradhan, and M. Lipson, "Micrometre-scale silicon electro-optic modulator," *Nature*, vol. 435, no. 7040, pp. 325–327, May 19, 2005.

[4] R. A. Soref, "Prospects for novel Si-based optoelectronic devices: Unipolar and p-i-p-i lasers," *Thin Solid Film*, vol. 294, pp. 325–329, 1997.

[5] V. R. Almeida, C. A. Barrios, R. R. Panepucci, and M. Lipson, "All-optical control of light on a silicon chip," *Nature*, vol. 431, no. 7012, pp. 1081–1084, Oct. 28, 2004.

[6] H. Ng, M. R. Wang, D. Li, X. Wang, J. Martinez, R. R. Panepucci, and K. Pathak, "1 × 4 wavelength reconfigurable photonic switch using thermally tuned microring resonators rabricated on silicon substrate," *IEEE Photon. Technol. Lett.*, vol. 19, no. 9, pp. 704–706, May 1, 2007.

[7] V. R. Almeida, R. R. Panepucci, and M. Lipson, "Nanotaper for compact mode conversion," *Opt. Lett.*, vol. 28, no. 15, pp. 1302–1304, 2003.

[8] M. S. Nawrocka, T. Liu, X. Wang, and R. R. Panepucci, "Tunable silicon microring resonator with wide free spectral range," *Appl. Phys. Lett.*, vol. 89, no. 7, pp. 071110–071113, Aug. 2006.